PLOS COMPLEX SYSTEMS

RESEARCH ARTICLE

Evaluating brain electroencephalogram signal dynamics across cognitive disorders using information geometry

Heng Jie Choong[1]*, **Eun-jin Kim**[1], **Fei He**[2]

1 Centre for Fluid and Complex Systems, Coventry University, Coventry, United Kingdom, **2** Centre for Computational Science and Mathematical Modelling, Coventry University, Coventry, United Kingdom

* choongh2@uni.coventry.ac.uk

OPEN ACCESS

Citation: Choong HJ, Kim E-j, He F (2025) Evaluating brain electroencephalogram signal dynamics across cognitive disorders using information geometry. PLOS Complex Syst 2(7): e0000059. https://doi.org/10.1371/journal.pcsy.0000059

Editor: Kimberly Glass, Brigham and Women's Hospital, UNITED STATES OF AMERICA

Received: November 19, 2024

Accepted: July 2, 2025

Published: July 31, 2025

Peer Review History: PLOS recognizes the benefits of transparency in the peer review process; therefore, we enable the publication of all of the content of peer review and author responses alongside final, published articles. The editorial history of this article is available here: https://doi.org/10.1371/journal.pcsy.0000059

Data availability statement: The data used in this work are available through the following

Abstract

Dementia, including Alzheimer's disease and frontotemporal dementia, is a progressive brain disorder that disrupts memory, thinking, and behavior, with early diagnosis being critical for effective intervention. This study examines the alteration of brain activity caused by dementia by analyzing electroencephalogram (EEG) signals using an information geometry method known as information rate, which captures the evolving patterns of brain signals over time rather than relying on static averages. This method is applied across standard EEG frequency bands – delta, theta, alpha, beta, and gamma – in participants with dementia and healthy controls. The characteristics of the distribution of information rate are studied through the statistical moments (such as mean, variance, skewness, and kurtosis) and Shannon entropy. The statistical comparisons are accessed using the Kruskal-Wallis test with Dunn's post-hoc analysis, and results are compared against a conventional average-base method using Jensen-Shannon distance. The results show that dynamic features of EEG signals – particularly in the theta, alpha, and beta bands – effectively distinguish Alzheimer's patients from healthy individuals, while the Shannon entropy of signal dynamics in frontal region differentiates frontotemporal dementia patients across the theta to gamma bands. Moreover, changes in the occipital region detected by information rate, but not by traditional method, further highlight the importance of capturing temporal variability. The method also successfully distinguishes individuals with Mild Cognitive Impairment from healthy controls, which conventional analysis failed to achieve. These results suggest that analyzing the dynamics properties of the brain signals provides a more sensitive and informative approach for identifying and distinguishing various forms of dementia.

Author summary

In this paper, we introduce a method called information rate to evaluate the dynamics of EEG signals. This method quantifies signals collectively within a dimensionless statistical

links: 1. 1st dataset: https://openneuro.org/datasets/ds004504/versions/1.0.8, which also referenced by the DOI https://doi.org/10.3390/data8060095. 2. 2nd dataset: https://misp.mui.ac.ir/en/eeg-data-0. Details about both datasets are available at the respective links. A summary of the datasets is also included in the manuscript to ensure the work is self-contained. The code used in this study is available on GitHub: https://github.com/sajtarius/info_geo_plos.

Funding: This work was supported by UK Research and Innovation under the EPSRC grant EP/X020193/1, awarded to Fei He (https://gtr.ukri.org/projects?ref=EP%2FX020193%2F1). The funder had no role in study design, data collection and analysis, decision to publish, or preparation of the manuscript.

Competing interests: The authors have declared that no competing interests exist.

space, whereas conventional methods tend to focus on either single signal or pairwise comparisons between signals. We compare information rate with an average-based approach, Jensen-Shannon distance, which samples the statistical space over time to enable pairwise comparisons between regions of interest across the EEG signals. To validate our findings, we performed Kruskal-Wallis and Dunn's statistical tests. Our results indicate that the information rate successfully differentiates healthy participants from patients with cognitive disorder (Alzheimer's, frontotemporal dementia, and Mild Cognitive Impairment). Furthermore, the dynamic analysis using information rate reveals distinctions between healthy and cognitively impaired groups at specific frequency bands in particular brain regions, a differences that the Jensen-Shannon distance does not capture.

Introduction

Dementia is a syndrome that refers to an individual who suffers from the loss of cognitive abilities involved in language, visual-spatial, executive and others. The loss of cognitive function would eventually cause the impairment of the functional abilities in coping with day-to-day life, like self-care, and lead to the death of the individual. There are several types of dementia, which generally include Alzheimer's disease, frontotemporal dementia, etc. Alzheimer's disease is distinct from other types of dementia by the high accumulation of amyloid plaques and tau tangles within the brain. Depending on the severity of the affected patients, they would lose their memory, which eventually leads to behavioural change and lose the ability to communicate. On the other hand, patients suffering from frontotemporal dementia would have a high accumulation of tau and TDP-43 protein in the frontal and temporal lobes. Similar to Alzheimer's disease, frontotemporal dementia patients would have the syndrome of behavioural change and difficulty in communication and movement [1–3]. Both Alzheimer's and frontotemporal dementia commonly involve lesions in the frontal and temporal regions, leading to personality changes. In the case of Alzheimer's, lesions in the parietal region may also occur in the early state, impairing somatosensory processing and spatial awareness [4].

Electroencephalography (EEG) is a non-invasive technique that records the electrical activity from the scalp through metal electrodes and conductive medium. Essentially, EEG records the electrical potentials generated by neuron activity in the brain, specifically from the cerebral cortex. These brain waves are high-frequency time series that consist of five main frequency bands: delta (0.5 to 5 Hz), theta (5 to 8 Hz), alpha (8 to 13 Hz), beta (13 to 32 Hz), and gamma (>32 Hz). Depending on the state of the participant, certain frequency bands would dominate the EEG, which can be used to identify the state of the brain. Delta band is associated with sleep, theta is associated with deep relaxation and inward focus, alpha is associated with a very relaxed state with passive attention, beta is associated with active external attention, and gamma is associated with the brain in a state of concentration [5,6].

In general, it is complicated to accurately diagnose the patients who suffer from specific categories of dementia. A variety of imaging modalities can be used for diagnosing dementia. For instance, fMRI offers high spatial resolution on the order of millimeters and is a reliable non-invasive tool, as Alzheimer's patients tend to show decreased activity in the hippocampal or parahippocampal regions during the encoding of new information [7–9]. EEG, on the other hand, provides high temporal resolution capable of capturing brain activity on the millisecond scale and has also been shown to be a reliable tool for studying the mental states of patients [9–11]. While fMRI provides better spatial resolution than EEG, it is generally

more expensive and less accessible for routine data acquisition [12]. Several studies suggested that EEG can generally be a good preliminary biomarker in diagnosing dementia patients. Patients who suffer from dementia tend to have the signals oscillate in lower frequencies than the normal healthy person due to the loss of synapses within the brain [13,14]. Claus et al. have shown that patients who suffered from Alzheimer's disease would have a decrease in alpha and beta activity shown in the spectra of EEG [15,16]. Besides, Jelic et al. also show that the relative power of alpha and theta bands are the important indicators for identifying Alzheimer's patients and mean frequency from the left temporal-occipital region are able to identify mild cognitively impaired patients with an accuracy of 85% [15,17].

In this work, a method known as information rate is employed to quantify the fluctuations and dynamics within the signals. Information rate is an information geometry method that quantitatively studies the evolution of time-dependent probability distributions [18,19]. This technique is a model-free method capable of quantifying non-linear, non-Gaussian stochasticity, and non-stationary, time-varying signals, but it also provides an alternative approach to evaluate signals as an ensemble across regions of interest [20]. Unlike conventional methods that focus on individual signals or pairwise comparisons (such as Hjorth parameters or entropy approaches like approximate entropy, fuzzy entropy, permutation entropy, phase entropy, or distribution entropy), this technique captures the collective dynamics within a specified region [21–27]. Generally, the evaluation of signal fluctuations is conducted using the sliding window approach. At each window, the signals are collected to estimate the distribution at each time point, and the comparison of two adjacent distributions yields the information rate. In this context, the distribution is sampled based on the amplitudes of an ensemble of EEG signals. To further understand the dynamics of the signals, the information rate is sampled to form a distribution, and the statistical moments, along with Shannon entropy derived from this distribution, provide insights into how the signals evolve.

Numerous studies have investigated the EEG correlates associated with dementia and related disorders. Generally speaking, in neurodegenerative disorders and related brain states with reduced levels of consciousness, there is a loss of complexity, sometimes characterised in terms of the emergence of slow rhythms (e.g., slow-wave sleep and enhanced theta activity) [28–33]. A complementary perspective on these characteristic differences is an increased complexity with arousal and attentive neuronal processing (e.g., event-related desynchronisation and induced gamma in the occipital regions) [34,35]. These descriptions suggest that in Alzheimer's disease and frontotemporal dementia, we would expect to see a reduced complexity or itinerancy in neuronal dynamics. This speaks to a reduction in the information rate of density dynamics. We, therefore, hypothesize a reduction in the mean and variance of information rates in these two groups of patients. In particular, we predict that the frontal regions should show a loss of itinerancy in terms of a reduced mean information rate — and its fluctuations as measured by higher-order statistical moments (such as variance). We anticipate that these differences would be expressed across frequency bands in a scale-invariant fashion. Furthermore, given the different regional specificities of frontotemporal dementia and Alzheimer's disease, we predict a complementary pattern of changes in the posterior brain regions, particularly the parietal, temporal and occipital regions.

To compare the differences between static and dynamic evaluations, pairwise comparisons of signals using Jensen-Shannon distance are conducted by evaluating the distribution of signals sampled across time. This distance measurement provides insight into the similarity between different brain regions, similar to correlation but emphasising distributional similarity. However, unlike the information rate, which captures time-evolving dynamics, the Jensen-Shannon distance does not incorporate time information, as the distribution reflects an aggregated view across time points. This approach enables a clear comparison

between static and dynamic perspectives, highlighting the unique insights provided by each method [36–38].

In the next section, the properties of the EEG signals will be discussed along with the filtering processes. The EEG signals are obtained through OpenNeuro, an open-source EEG database, which provides the post-processed signals for reproducibility [39]. Additional EEG data, consisting of Mild Cognitive Impairment (MCI) and healthy subjects, were used to validate the proposed analyses. These signals were obtained from Isfahan University of Medical Sciences and were preprocessed with all the steps stated within the text [40]. Next, the Jensen-Shannon distance and information rate are discussed in detail along with the parameters used in this work [18,19,41]. Following that, the statistical test based on the Jensen-Shannon distance and information rate is conducted through the Kruskal-Wallis test and Dunn's test as the post hoc [42]. These tests are used to evaluate the significant difference in the median between the groups of patients (e.g. Alzheimer's, frontotemporal dementia, and healthy patients), which are discussed briefly within this paper.

Materials and methods

EEG signals

The first EEG dataset used in this analysis was obtained from [39], which is freely available in OpenNeuro. The dataset comprises resting state EEG recordings from 88 subjects, including 36 with Alzheimer's disease (AD), 23 with frontotemporal Dementia (FTD), and 29 healthy controls (HC). Cognitive status was assessed using the Mini-Mental State Examination (MMSE), with the AD group exhibiting lower MMSE scores (mean = 17.75) compared to FTD (mean = 22.17) and HC (mean = 30) groups. Median disease duration was 25 months (Interquartile range: 24–28.5). No dementia-related comorbidities were reported in the AD group. Average ages were 66.4 (sd = 7.9) for AD, 63.6 (sd = 8.2) for FTD, and 67.9 (sd = 5.4) for CN.

The recordings were conducted at the 2nd Department of Neurology of AHEPA General Hospital in Thessaloniki using a Nihon Kohden EEG 2100 device, with 19 scalp electrodes placed according to the 10-20 international system. Two reference electrodes (A1 and A2) were used to check impedance. During the recordings, participants were seated with eyes closed, adhering to clinical protocol. The sampling rate was 500 Hz with 10μV/mm resolution, utilizing anterior-posterior bipolar and referential montage with Cz electrode as the common reference. Recordings lasted approximately 13.5 minutes for AD (min = 5.1, max = 21.3), 12 minutes for FTD (min = 7.9, max = 16.9), and 13.8 for CN (min = 12.5, max = 16.5), totalling 485.5 minutes of AD, 276.5 minutes of FTD, and 402 minutes of CN recordings included in the dataset.

Prior to the analysis, the EEG was preprocessed by applying a Butterworth band-pass filter (0.5–45 Hz) and re-referencing signals to A1-A2 electrodes. Artifact Subspace Reconstruction (ASR) was then used to remove segments of data with artifacts exceeding a maximum acceptable window of 0.5 seconds and a standard deviation cutoff of 17. Next, Independent Component Analysis (ICA) was performed to transform the 19 EEG signals into 19 ICA components. Components classified as "eye artifacts" or "jaw artifacts" by the ICLabel routine in the EEGLAB platform were automatically rejected. Despite the recordings being in a resting state with eyes closed, some eye movement artifacts were still present.

The second EEG dataset, obtained from [40] and also used in [43], was used to validate the methods applied in this study. It includes scalp EEG recordings from 34 subjects aged 60 to 77 years, comprising 16 healthy controls (HC) and 18 patients with Mild Cognitive Impairment

(MCI). Cognitive status was assessed using Petersen's criteria, the Mini-Mental State Examination (MMSE), and the Neuropsychiatry Unit Cognitive Assessment Tool (NUCOG). In the MMSE, the HC group scored above 26, while MCI participants scored between 21 and 26.

Recordings were conducted at Sina and Nour Hospitals in Isfahan, Iran, with approval from the Deputy of Research and Technology at Isfahan University of Medical Sciences. EEG signals were acquired using a 32-channel Galileo NT device (EBNeuro, Italy) with 19 electrodes placed according to the international 10–20 system. Data were sampled at 256 Hz, and electrode impedance was maintained below 5 kΩ. All recordings were performed during eyes-closed resting-state sessions and lasted 30 minutes.

The dataset was first converted to the BIDS format and then preprocessed. The preprocessing pipeline mirrored that of the first dataset. Signals were resampled to 500 Hz to match the sampling rate of the first dataset. A Butterworth band-pass filter (1–100 Hz) and a 50 Hz notch filter were applied to remove power line interference common in Iran. Signals were also detrended to eliminate DC offsets. ASR was applied using a maximum window duration of 0.5 seconds and a standard deviation cutoff of 2.5 to eliminate segments with excessive noise.

Independent Component Analysis (ICA) was then performed using the Extended Infomax algorithm with 18 components. This algorithm is capable of identifying both super-Gaussian and sub-Gaussian sources, typically associated with ocular and muscular artifacts, respectively [44]. Artifactual components were identified and labelled using the `mne-icalabel` package. However, it should be noted that the package may not detect all artifact-related components, and some residual artifacts may persist in the filtered signals. Common Average Referencing (CAR) was not applied, as it may amplify existing artifacts and obscure neural signals.

Jensen-Shannon distance

To evaluate the difference between two probability distributions, Kullback-Leibler (KL) divergence/relative entropy is commonly used, but it is not symmetric; hence, it cannot be used as a metric. On the other hand, Jensen Shannon (JS) distance is a metric that quantifies the difference between two probability distributions [19,41]. For two distributions (P and Q), JS distance is defined as follows.

$$JS(P||Q) = \sqrt{\frac{1}{2}\left(KL(P||M) + KL(Q||M)\right)}. \tag{1}$$

Here, $M = \frac{1}{2}(P + Q)$ is known as mixture distribution and $KL(P||M) = \sum P \log \frac{P}{M}$ is the KL divergence between the distributions P and M. It is trivial that a small JS would indicate that the given distributions are relatively similar to each other and vice versa.

In this work, JS distance is used to evaluate the similarity between the amplitude of EEG signals measured in the different brain regions. Typically, the amplitude of the signal is sampled throughout the time, and the distribution is estimated within the range of $-100\mu V$ to $100\mu V$, which are the minimum and maximum of the amplitude range of the provided signals. Subsequently, a symmetric JS distance matrix is expected as shown in Fig 1.

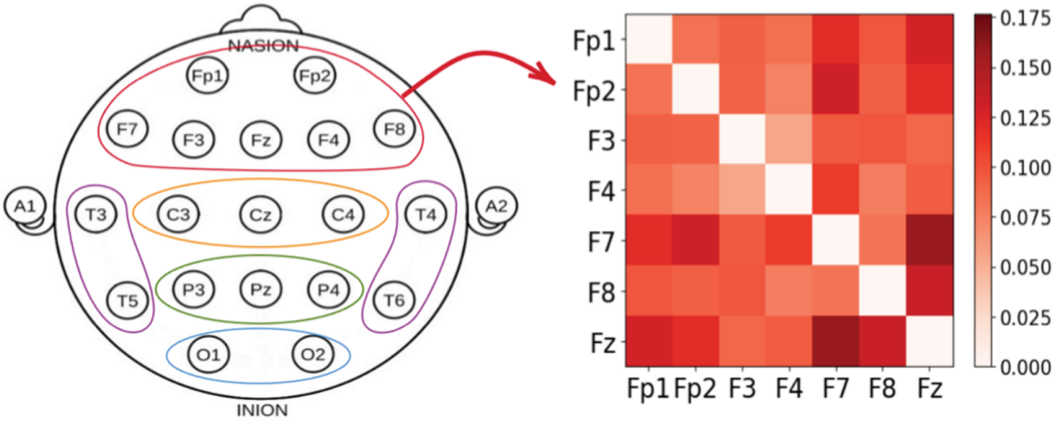

Fig 1. JS distance matrix between the electrodes at the frontal region for a single participant.

https://doi.org/10.1371/journal.pcsy.0000059.g001

Information rate

The state of the brain captured by the EEG is represented as time series signals. Depending on the activity of the brain at the specific region, the fluctuation of the signals would be varied. These fluctuations can be evaluated and studied in the dimensionless statistical manifold, known as probability distribution, by collecting the signals from regions of interest and evaluating them using Kullback-Leibler (KL) divergence. However, this measure is not symmetrical and not path-dependent. The time-dependent changes in the probability distribution ($p(x,t)$) over measured brain states can be thought of as a path or movement on a statistical manifold, where each point on the manifold corresponds to a probability distribution. The information rate ($\Gamma(t)$) scores the rate of change of information distance with movement on the statistical manifold. Technically, this can be measured as a path integral of infinitesimal differences in probability distributions, as measured with (a function of) the KL divergence. This information rate ($\Gamma(t)$) reduces to a simple expression — in terms of the rate of change of the probability distributions as described below — and captures the density dynamics in a way that static measures do not. It is this density dynamics that underwrites the complexity and itinerancy of transitions through successive brain states.

$$\Gamma^2(t) = 4 \int dx \left[\partial_t \sqrt{p(x,t)}\right]^2 . \tag{2}$$

In this work, the information rate of the EEG signals is evaluated based on a group of signals from specific channels of interest instead of a single signal. The evolution of the distribution is sampled through the sliding window approach. The window size is determined by the mean of the reciprocal of the frequencies in the bands of interest, with a 50% overlap between the consecutive windows. For instance, for delta band (0.5 to 5 Hz), the window size is chosen to be $\left(\frac{1}{0.5} + \frac{1}{5}\right) * 0.5$ secs = 1.1 secs ensuring that the collected signals accurately represent the complexity of the signals. The 50% overlap helps reduce the impact of noise when computing the information rate. At each window, measured in seconds (e.g., 1.1s for the delta band), the distribution is estimated via histogram with the bin size determined by Rice rule [45]. Note that the range of the distribution is sampled based on the maximum and minimum of the signals' amplitude at two consecutive windows in order to evaluate the complexity of the signal well.

The details of the numerical computation of the information rate are as follows. Consider a discrete time series with length n, consisting of c number of channels: $\boldsymbol{x}_{c,n\in\mathbb{N}}$. The signals $\boldsymbol{x}_{c,n\in\mathbb{N}}$ are divided into segments with a window size of ε and overlap of τ resulting in $\boldsymbol{x}_{c,T\in\mathbb{N}}^{(\varepsilon),(\tau)\in\mathbb{N}}$, where $T = \left\lfloor \frac{n-\varepsilon}{\varepsilon-\tau} \right\rfloor + 1$. Each window would have $c \times \varepsilon$ of data points, and the distribution is estimated via histogram with the bin size (n_{hist}) determined using Rice rule [45]:

$$n_{\text{hist}} = \left\lceil 2(c \times \varepsilon)^{\frac{1}{3}} \right\rceil. \tag{3}$$

With each window of data points sampled, a series of probability distributions is expected, denoted as $\boldsymbol{P}\left(\boldsymbol{x}_{c,T}^{(\varepsilon),(\tau)}\right)_{n_{\text{hist}},T\in\mathbb{N}}$. It should be noted that in this work, the range of the distribution is not fixed for the entire series of the calculations but is instead based on the maximum and minimum values with two consecutive windows of data points. This ensures the given data points are well sampled to form the distribution.

Utilizing the series of probability distributions, the information rate is computed to quantify the rate of change of the distribution as defined in Eq (2). Numerically, the information rate ($\boldsymbol{\Gamma}(T)$) is computed based on the following expression:

$$\begin{aligned}
\boldsymbol{\Gamma}^2(T) &= 4\sum_X \frac{\Delta \boldsymbol{X}}{\Delta \boldsymbol{I}^2}\left[\sqrt{\boldsymbol{P}\left(\boldsymbol{x}_{c,T}^{(\varepsilon),(\tau)}\right)_{X,I_n}} - \sqrt{\boldsymbol{P}\left(\boldsymbol{x}_{c,T}^{(\varepsilon),(\tau)}\right)_{X,I_{n-1}}}\right]^2,\\
\boldsymbol{X} &= \left\{\min\left(\boldsymbol{x}_{c,T=I_n}^{(\varepsilon),(\tau)}, \boldsymbol{x}_{c,T=I_{n-1}}^{(\varepsilon),(\tau)}\right), \cdots, \max\left(\boldsymbol{x}_{c,T=I_n}^{(\varepsilon),(\tau)}, \boldsymbol{x}_{c,T=I_{n-1}}^{(\varepsilon),(\tau)}\right)\right\}, |\boldsymbol{X}| = X = n_{\text{hist}},\\
\boldsymbol{I} &= \{\text{sampling frequency} * I_n * (\varepsilon - \tau)\}, I_n \in [0, T] \in \mathbb{N}, n \in \mathbb{N}, |\boldsymbol{I}| = T.
\end{aligned} \tag{4}$$

To quantitatively study the degree of change in the distribution, the distribution of the information rate ($P(\boldsymbol{\Gamma}(T))$) is estimated, and Shannon entropy ($H(\Gamma)$) of the information rate is computed with the following expression:

$$H(\Gamma) = -\sum_{\boldsymbol{\Gamma}} P(\boldsymbol{\Gamma}(T)) \ln P(\boldsymbol{\Gamma}(T)). \tag{5}$$

To further quantify the distribution, first moment (M_1) and second to fourth cumulants ($M'_{n\in[2,4]}$) are also used in this work to evaluate the shape of the information rate distribution. The first moment measures the central tendency of the distribution. The second cumulant, variance, quantifies the dispersion of values around the mean. The third cumulant, skewness, measures the asymmetry of the distribution. And the fourth cumulant, kurtosis, quantifies the "tailedness" of the distribution.

$$\text{average} = \mu = \sum_{\boldsymbol{\Gamma}} \boldsymbol{\Gamma}(T)\, P(\boldsymbol{\Gamma}(T)), \tag{6}$$

$$\text{Variance} = M'_2 = \sum_{\boldsymbol{\Gamma}} (\boldsymbol{\Gamma}(T) - \mu)^2\, P(\boldsymbol{\Gamma}(T)), \tag{7}$$

$$\text{Skewness} = M'_3 = \frac{1}{\sigma^3}\sum_{\boldsymbol{\Gamma}} (\boldsymbol{\Gamma}(T) - \mu)^3\, P(\boldsymbol{\Gamma}(T)), \tag{8}$$

$$\text{Kurtosis} = M'_4 = \frac{1}{\sigma^4}\sum_{\boldsymbol{\Gamma}} (\boldsymbol{\Gamma}(T) - \mu)^4\, P(\boldsymbol{\Gamma}(T)), \tag{9}$$

where $\sigma = \sqrt{M'_2}$ is the standard deviation. The entire process of computing the information rate, along with its statistical descriptors, is illustrated in Fig 2.

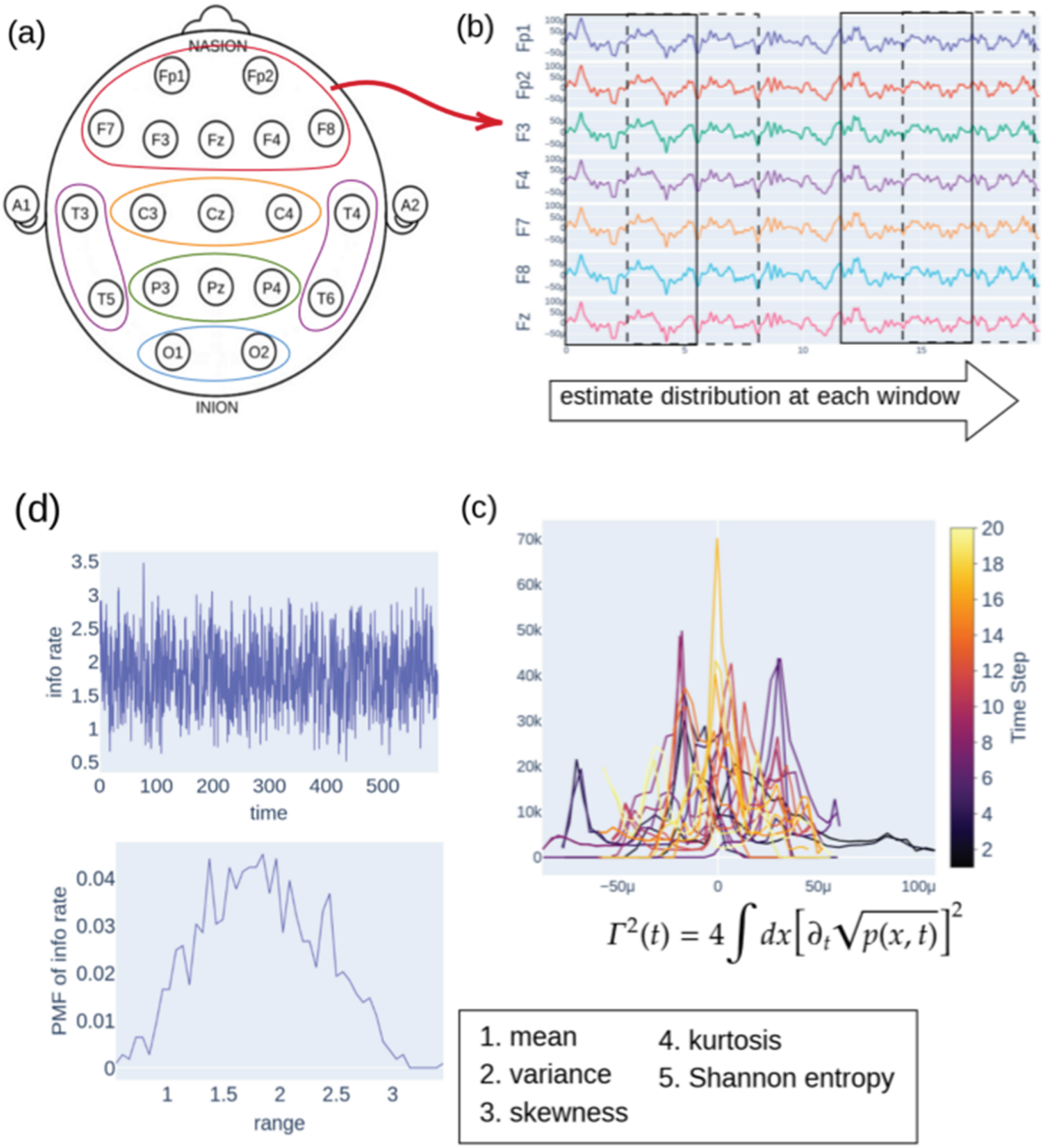

Fig 2. The procedure of information rate. (a) Selection of electrodes based on the region of interest. (b) Application of sliding window approach to estimate the distribution within each window. (c) Quantification of distribution evolution using information rate ($\Gamma(t)$) to assess dynamic changes in signal behaviour as an ensemble of the region of interest. (d) Estimation of the distribution based on information rate, followed by evaluation of statistical moments (mean, variance, skewness, and kurtosis) and Shannon entropy, which are then subjected to the Kruskal-Wallis and Dunn's statistical tests.

https://doi.org/10.1371/journal.pcsy.0000059.g002

Kruskal-Wallis test

Kruskal-Wallis test is a non-parametric statistic test that quantitatively evaluates the significant differences between the medians of three or more independent groups of data. This test is

a non-parametric alternative to the one-way ANOVA, which evaluates the significant differences between the means of three or more groups, meaning it does not require the assumptions of normal distribution and equal variances (homoscedasticity) for each group. The Kruskal-Wallis test first ranks all the data and then compares the sum of the ranks between the groups. The test statistic H is calculated with the following expression [42]:

$$H = \frac{12}{N(N+1)} \sum_{i=1}^{k} \frac{R_i^2}{n_i} - 3(N+1). \tag{10}$$

Here, in reference to the first dataset, $N = 88$ is the total number of observations for all the groups; $k = 3$ is the number of groups; $n_{i\in[1,3]} = \{36, 23, 29\}$ is the number of observations in the i-th group; R_i is the sum of the ranks for the i-th group. Note that $i = 1$ refers to the Alzheimer's group, $i = 2$ refers to the frontotemporal dementia group, and $i = 3$ refers to the healthy control group.

The calculated statistic is compared with the chi-square distribution with k–1 degrees of freedom to reveal the significant difference (A p-value <0.05 was considered statistically significant). This test identifies the presence of a significant difference among the groups but does not indicate which specific groups show the difference.

To identify which specific group(s) show significant differences, post hoc Dunn's test is conducted after the Kruskal-Wallis test indicates significant differences. Dunn's test (Z_{ij}) is a non-parametric multiple comparison procedure that compares the mean rank differences between the pairs of the groups, For instance, for groups i and j, it is expressed as $Z_{ij} = \frac{\frac{R_i}{n_i} - \frac{R_j}{n_j}}{\sqrt{\frac{N(N+1)}{12}\left(\frac{1}{n_i} + \frac{1}{n_j}\right)}}$. Here, in reference to the first dataset, $R_{i,j\in[1,3]}$ represents the sum of the ranks for the i-th or j-th group; $n_{i,j\in[1,3]} = \{36, 23, 29\}$ is the number of observations in the i-th or j-th group; $N = 88$ is the total number of observations for all the groups. Note here again that $i = 1$ refers to the Alzheimer's group, $i = 2$ refers to the frontotemporal dementia group, and $i = 3$ refers to the healthy control group. To account for the family-wise error rate in multiple pairwise comparisons, the Holm-Bonferroni correction is applied in this work since there are only 3 groups with a total of 88 participants data. This method adjusts the p-value in a stepwise manner by first ordering the p-value from smallest to largest and multiplying them by a factor of $(m + 1 - r)$, where $m = 3$ is the number of comparisons and r is the rank of the order [46,47].

Software and libraries

All code was written in `Python` and executed using `Python 3.9.13`. `MNE-Python 1.8.0` was used to read and filter the EEG into different frequency bands. The `asrpy` package was used to perform ASR, and `mne-icalabel 0.7.0` was employed to identify and label independent components associated with artifacts for ICA. `SciPy 1.13.1` was employed to calculate the Jensen-Shannon distance and perform the Kruskal-Wallis test. For post hoc analysis, Dunn's test was conducted using `Scikit-posthocs 0.9.0`. Interactive visualizations were created by using `Plotly 5.18.0`. `Joblib 1.1.0` was used to parallelize the computations for information rate calculation. The complete code is available at https://github.com/sajtarius/info_geo_plos.

Results

Kruskal-Wallis test Jensen-Shannon distance between channels

As noted above, following the evaluation of the Jensen-Shannon distance between the signals for each electrode combination across all participants, the distances were compiled for statistical analysis using the Kruskal-Wallis test. This test was employed to quantitatively determine which combinations of distances exhibited statistically significant differences between groups, as illustrated in Fig 3. The results of the Kruskal-Wallis test on the Jensen-Shannon distance for each brain region are presented in Table 1. The first column of the table indicates the number of electrode combinations within each region, calculated using the binomial coefficient formula: $C(n,r) = \frac{n!}{r!(n-r)!}$ where n represents the number of electrodes in the region of interest, and r ($r = 2$ in this case) corresponds to the number of samples for pairwise comparisons of the Jensen-Shannon distance between electrodes. Subsequent columns report the number of significant differences identified through the Kruskal-Wallis test, as well as the corresponding percentages. For instance, in the frontal region within the 0.5 to 5 Hz frequency band, five combinations were found to exhibit statistically significant differences, as shown in S1 Fig, corresponding to 5/21 or 28.81%.

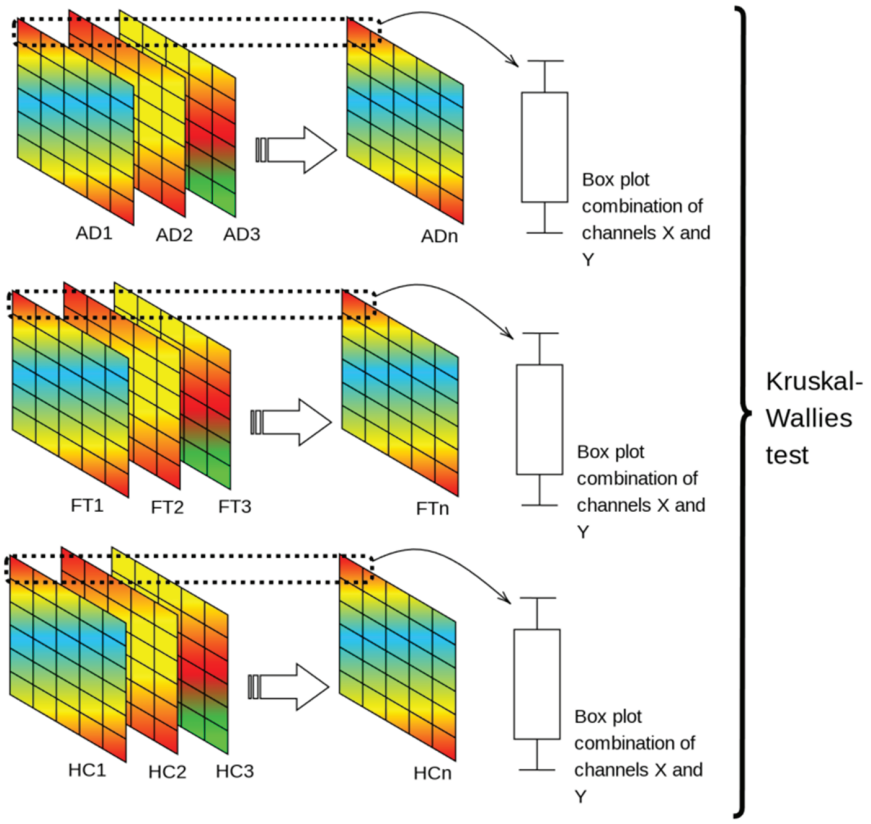

Fig 3. The procedure of Kruskal-Wallis test was done on Jensen-Shannon distance values of Alzheimer's (AD), frontotemporal dementia (FT), and healthy control (HC) groups. For each participant, the Jensen-Shannon distance between different electrodes of EEG is evaluated based on the distribution sampled throughout the time. For a specific combination, the Kruskal-Wallis test was conducted after the data was collected with respect to each group.

https://doi.org/10.1371/journal.pcsy.0000059.g003

Table 1. Number of combination of channels that show significant different after Kruskal-Wallis test of Jensen-Shannon distance. The result is based on the first dataset that consists of Alzheimer's, frontotemporal dementia, and Healthy subjects [39].

region (#)	delta (%)	theta (%)	alpha (%)	beta (%)	gamma (%)
F ($C(7,2) = 21$)	5 (28.81)	12 (57.14)	0 (0)	0 (0)	3 (14.29)
C ($C(3,2) = 3$)	1 (33.33)	0 (0)	0 (0)	0 (0)	0 (0)
P ($C(3,2) = 3$)	1 (33.33)	0 (0)	1 (33.33)	1 (33.33)	0 (0)
O ($C(2,2) = 2$)	0 (0)	0 (0)	0 (0)	0 (0)	0 (0)
T ($C(4,2) = 6$)	0 (0)	1 (16.67)	4 (66.67)	1 (16.67)	2 (33.33)

The labels of regions are F (Frontal and pre-frontal), C (Central), P (Parietal), O (Occipital), and T (Temporal), with each region containing 7, 3, 3, 2, and 4 electrodes, subsequently. The number of combinations for each region is indicated in the bracket. The frequency bands are shown at the top row and consist of the delta band (0.5 to 5 Hz), theta band (5 to 8 Hz), alpha band (8 to 16 Hz), beta band (16 to 32 Hz), and gamma band (32 to 100 Hz). The percentage values are included for reference (e.g. 5/21 = 28.81% for F region at 0.5 to 5 Hz). The results shown here are summarized from S1 Fig to S11 Fig in Supporting information.

https://doi.org/10.1371/journal.pcsy.0000059.t001

As summarized in Table 1, for the first dataset, none of the electrode combinations in the occipital region exhibited a statistically significant difference ($p<0.05$) across all frequency bands between Alzheimer's, frontotemporal, and healthy control groups. In contrast, the temporal region showed at least one significant combination from the theta band to the gamma band. Both the frontal and parietal regions exhibited significant differences in at least one combination of Jensen-Shannon distance across three frequency bands. In the central region, only the delta band revealed a significant difference in Jensen-Shannon distance for a single combination. The box plots illustrating these combinations are presented in Supporting information. Moreover, for the second dataset, no electrode combination showed a significant difference between the healthy and Mild Cognitive Impairment groups. Therefore, no table is included in the text.

Information rate and statistical test

To visualize the rate of change in signal complexity, the information rate for each participant across regions of interest (frontal, central, parietal, occipital, and temporal) and across all frequency bands is represented using probability mass functions (PMFs), as shown in S12 Fig to S18 Fig. Since each participant exhibits a unique distribution, the average (depicted by solid lines) and standard deviation (shaded regions) are included for all plots in S12 Fig to S18 Fig, allowing for a clear visual comparison of the variability in information rate distribution within each group. From these plots, higher variability in the information rate distributions can be observed in Alzheimer's and frontotemporal groups for the frontal, central, parietal, and temporal regions, whereas in the occipital region, healthy participants exhibit increased variability. To ensure meaningful comparisons across frequency bands and regions, PMFs in S12 Fig to S18 Fig were estimated using a bin size of 40.

To quantitatively assess these distributions, statistical moments (mean, variance, skewness, and kurtosis) were calculated for the PMFs as shown in S12 Fig to S18 Fig. For the first dataset, Figs 4, 5, 6, and 7 show box plots of the mean information rate for each group, while the variance is depicted in Figs 8, 9, and 10. Skewness, which measures the asymmetry of the distribution, is illustrated in Figs 11, 12, 13, and 14. Kurtosis, which reflects the extremity of the distribution values, is shown in Figs 15, 16, 17, and 18. In this study, skewness and kurtosis provide additional insights for distinguishing participant groups beyond mean and variance. Notably, skewness effectively differentiates all the participant groups, in the occipital region at the beta band, while the mean only distinguishes between Alzheimer's and healthy groups. In addition, Shannon entropy was computed as shown in Figs 19, 20, 21, and 22 to

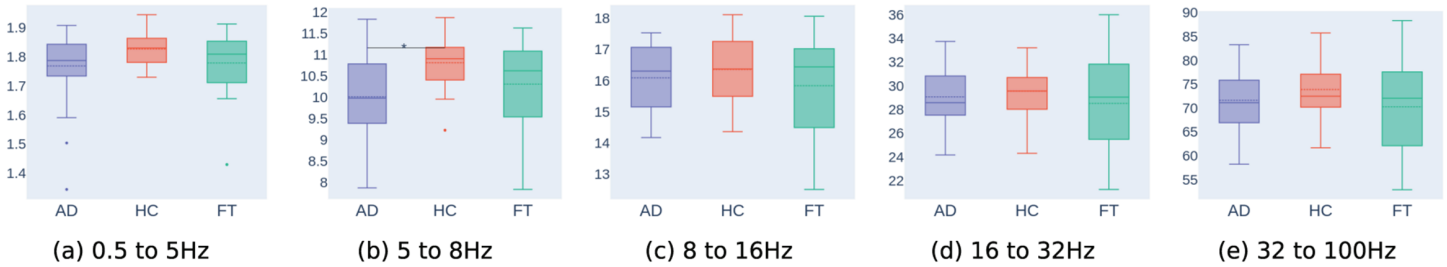

Fig 4. Box plot of the mean of the information rate distribution in the frontal region (AD: Alzheimer's disease; HC: healthy controls; FT: frontotemporal dementia). Significant differences ($p<0.05$) are indicated by "–*–".

https://doi.org/10.1371/journal.pcsy.0000059.g004

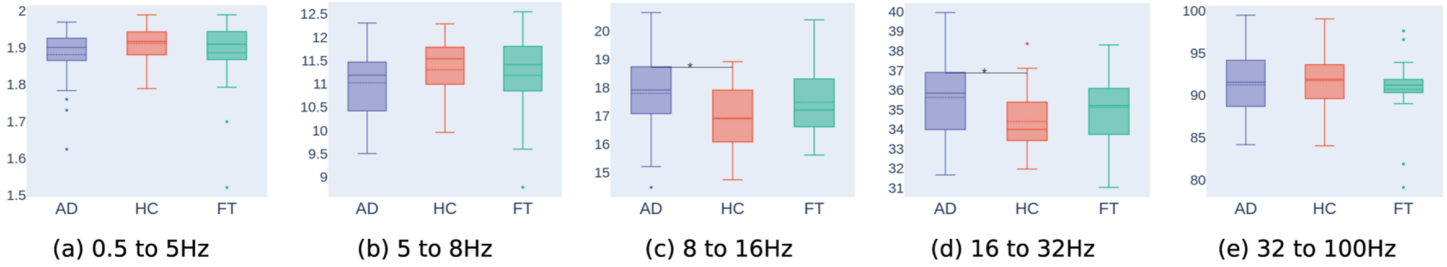

Fig 5. Box plot of the mean of the information rate distribution in the parietal region (AD: Alzheimer's disease; HC: healthy controls; FT: frontotemporal dementia). Significant differences ($p<0.05$) are indicated by "–*–".

https://doi.org/10.1371/journal.pcsy.0000059.g005

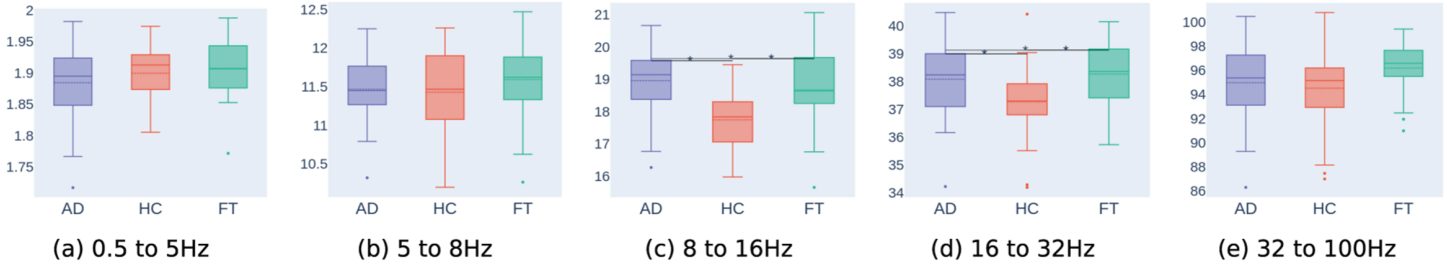

Fig 6. Box plot of the mean of the information rate distribution in the occipital region (AD: Alzheimer's disease; HC: healthy controls; FT: frontotemporal dementia). Significant differences ($p<0.05$) are indicated by "–*–".

https://doi.org/10.1371/journal.pcsy.0000059.g006

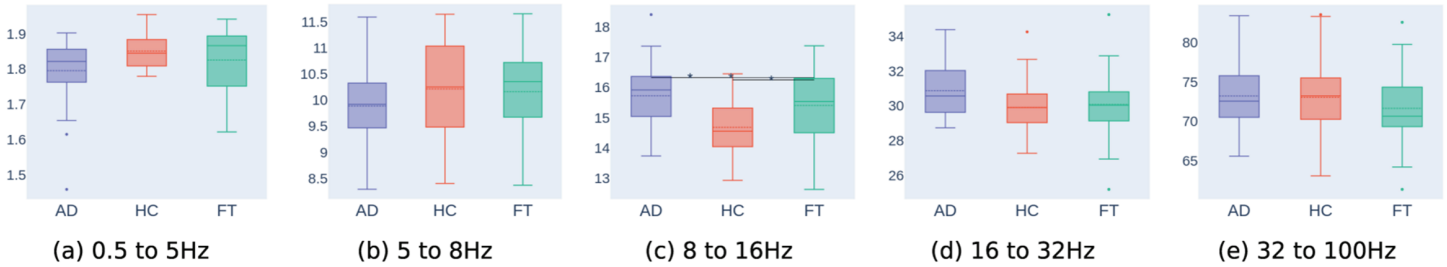

Fig 7. Box plot of the mean of the information rate distribution in the temporal region (AD: Alzheimer's disease; HC: healthy controls; FT: frontotemporal dementia). Significant differences ($p<0.05$) are indicated by "–*–".

https://doi.org/10.1371/journal.pcsy.0000059.g007

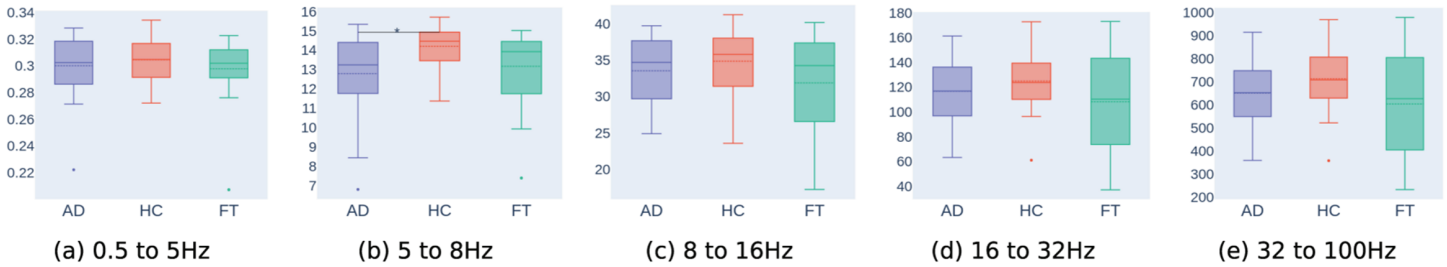

Fig 8. Box plot of the variance of the information rate distribution in the frontal region (AD: Alzheimer's disease; HC: healthy controls; FT: frontotemporal dementia). Significant differences ($p<0.05$) are indicated by "−*−".

https://doi.org/10.1371/journal.pcsy.0000059.g008

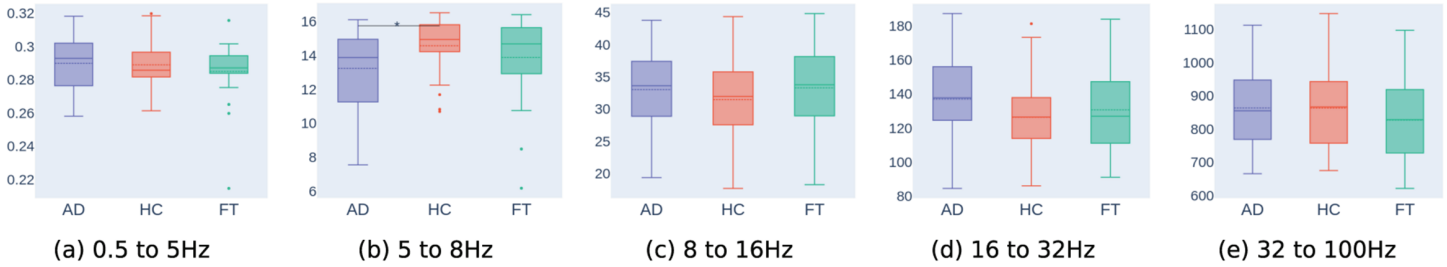

Fig 9. Box plot of the variance of the information rate distribution in the central region (AD: Alzheimer's disease; HC: healthy controls; FT: frontotemporal dementia). Significant differences ($p<0.05$) are indicated by "−*−".

https://doi.org/10.1371/journal.pcsy.0000059.g009

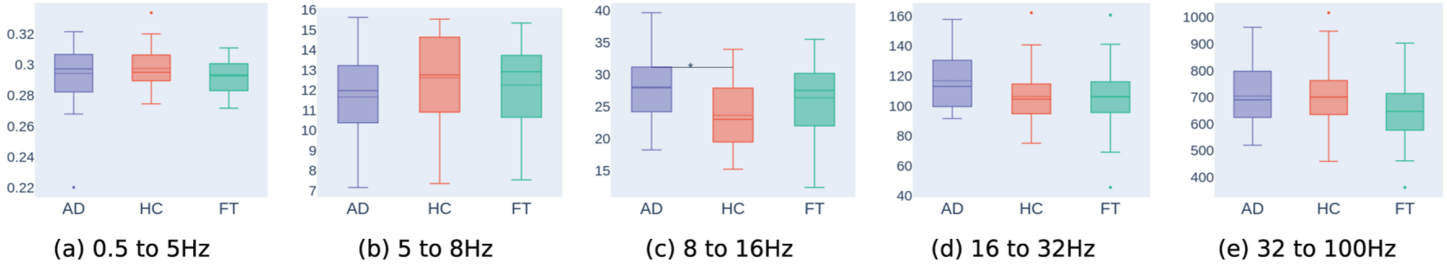

Fig 10. Box plot of the variance of the information rate distribution in the temporal region (AD: Alzheimer's disease; HC: healthy controls; FT: frontotemporal dementia). Significant differences ($p<0.05$) are indicated by "−*−".

https://doi.org/10.1371/journal.pcsy.0000059.g010

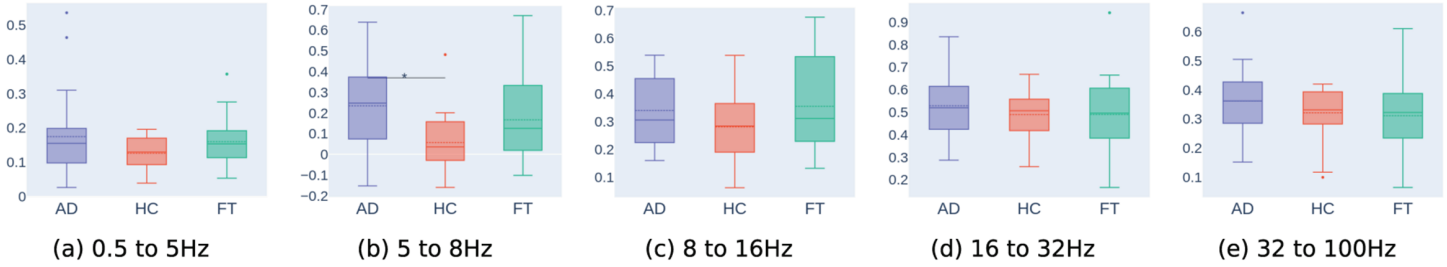

Fig 11. Box plot of the skewness of the information rate distribution in the frontal region (AD: Alzheimer's disease; HC: healthy controls; FT: frontotemporal dementia). Significant differences ($p<0.05$) are indicated by "−*−".

https://doi.org/10.1371/journal.pcsy.0000059.g011

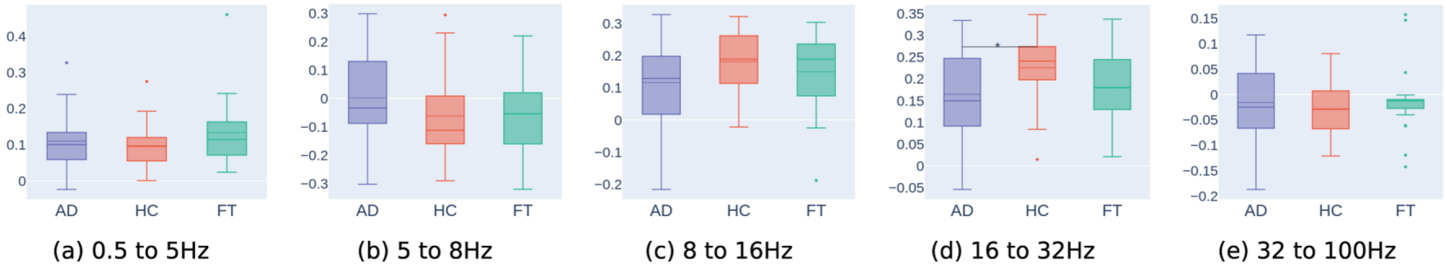

Fig 12. Box plot of the skewness of the information rate distribution in the parietal region (AD: Alzheimer's disease; HC: healthy controls; FT: frontotemporal dementia). Significant differences ($p<0.05$) are indicated by "–*–".

https://doi.org/10.1371/journal.pcsy.0000059.g012

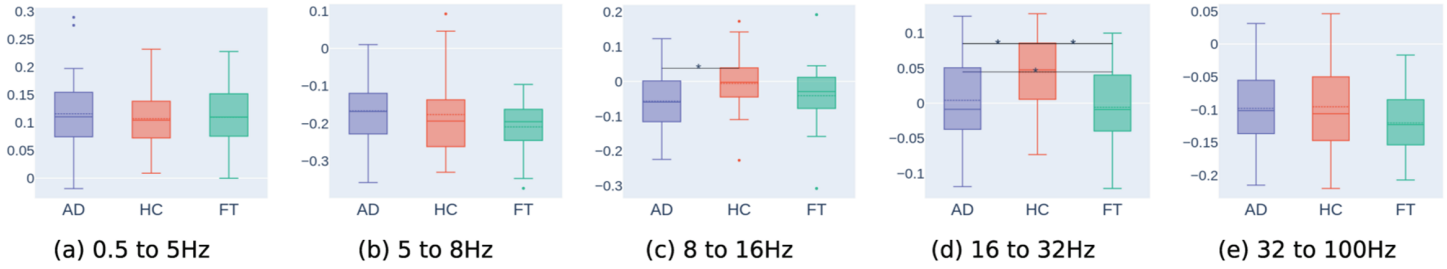

Fig 13. Box plot of the skewness of the information rate distribution in the occipital region (AD: Alzheimer's disease; HC: healthy controls; FT: frontotemporal dementia). Significant differences ($p<0.05$) are indicated by "–*–".

https://doi.org/10.1371/journal.pcsy.0000059.g013

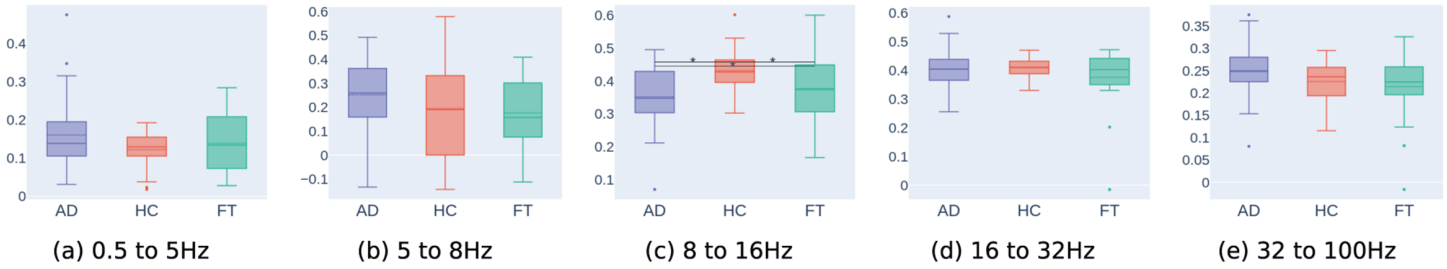

Fig 14. Box plot of the skewness of the information rate distribution in the temporal region (AD: Alzheimer's disease; HC: healthy controls; FT: frontotemporal dementia). Significant differences ($p<0.05$) are indicated by "–*–".

https://doi.org/10.1371/journal.pcsy.0000059.g014

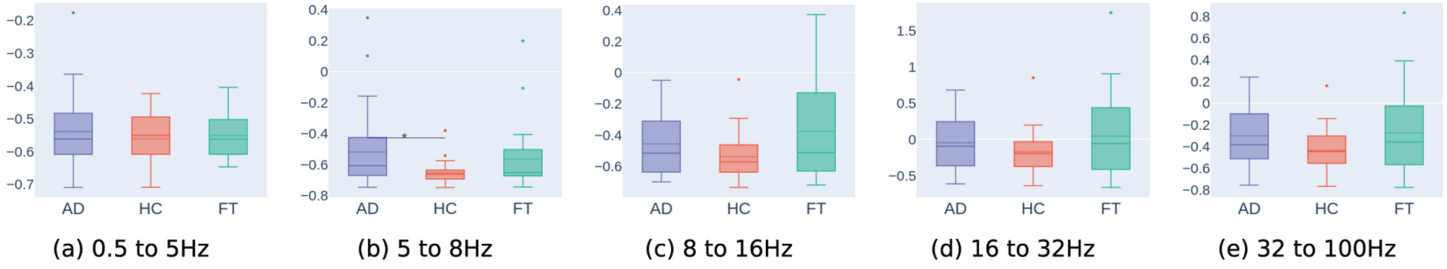

Fig 15. Box plot of the kurtosis of the information rate distribution in the frontal region (AD: Alzheimer's disease; HC: healthy controls; FT: frontotemporal dementia). Significant differences ($p<0.05$) are indicated by "–*–".

https://doi.org/10.1371/journal.pcsy.0000059.g015

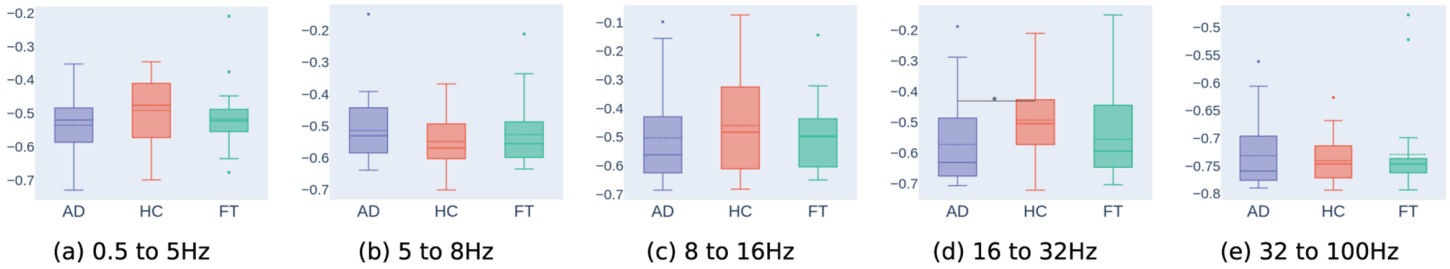

Fig 16. Box plot of the kurtosis of the information rate distribution in the parietal region (AD: Alzheimer's disease; HC: healthy controls; FT: frontotemporal dementia). Significant differences ($p<0.05$) are indicated by "–*–".

https://doi.org/10.1371/journal.pcsy.0000059.g016

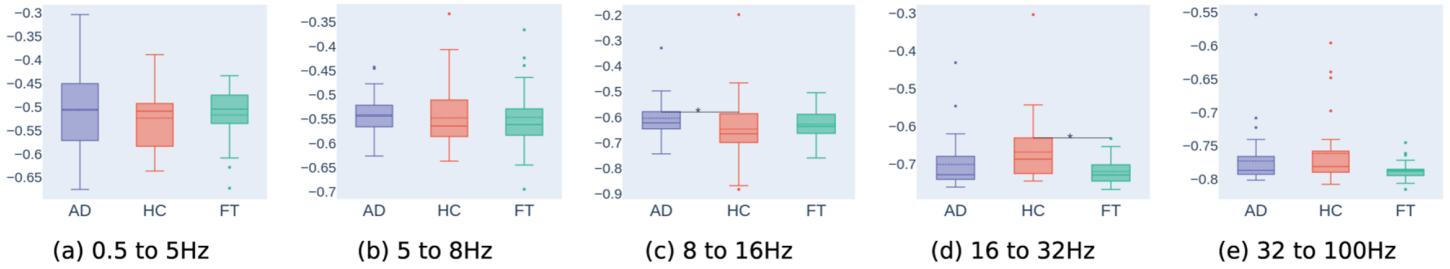

Fig 17. Box plot of the kurtosis of the information rate distribution in the occipital region (AD: Alzheimer's disease; HC: healthy controls; FT: frontotemporal dementia). Significant differences ($p<0.05$) are indicated by "–*–".

https://doi.org/10.1371/journal.pcsy.0000059.g017

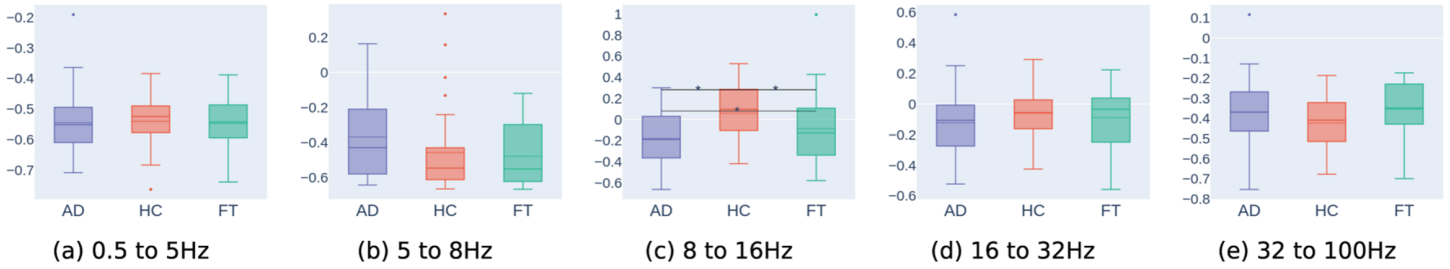

Fig 18. Box plot of the kurtosis of the information rate distribution in the temporal region (AD: Alzheimer's disease; HC: healthy controls; FT: frontotemporal dementia). Significant differences ($p<0.05$) are indicated by "–*–".

https://doi.org/10.1371/journal.pcsy.0000059.g018

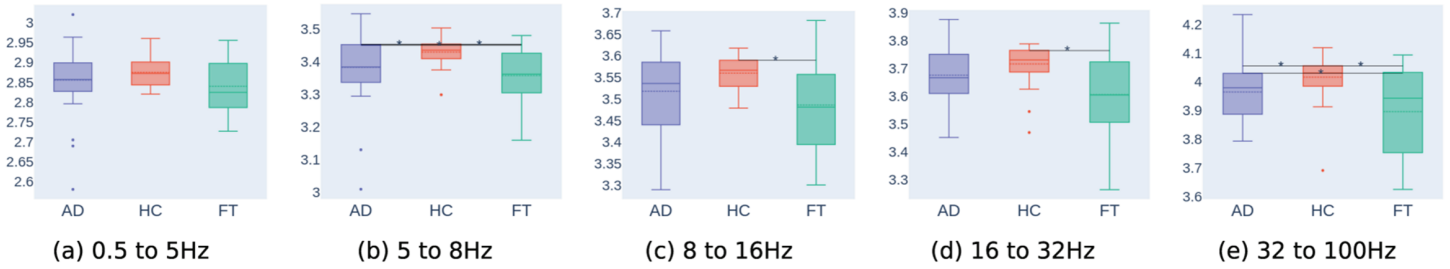

Fig 19. Box plot of the Shannon entropy of the information rate distribution in the frontal region (AD: Alzheimer's disease; HC: healthy controls; FT: frontotemporal dementia). Significant differences ($p<0.05$) are indicated by "–*–".

https://doi.org/10.1371/journal.pcsy.0000059.g019

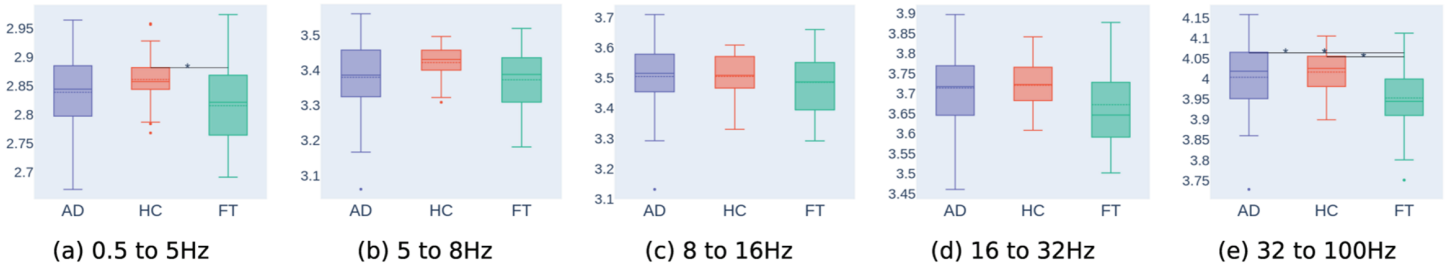

Fig 20. Box plot of the Shannon entropy of the information rate distribution in the central region (AD: Alzheimer's disease; HC: healthy controls; FT: frontotemporal dementia). Significant differences ($p<0.05$) are indicated by "–*–".

https://doi.org/10.1371/journal.pcsy.0000059.g020

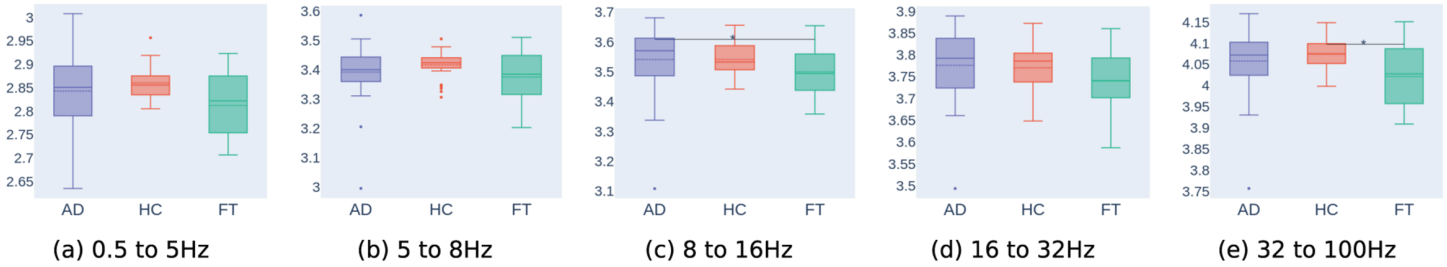

Fig 21. Box plot of the Shannon entropy of the information rate distribution in the parietal region (AD: Alzheimer's disease; HC: healthy controls; FT: frontotemporal dementia). Significant differences ($p<0.05$) are indicated by "–*–".

https://doi.org/10.1371/journal.pcsy.0000059.g021

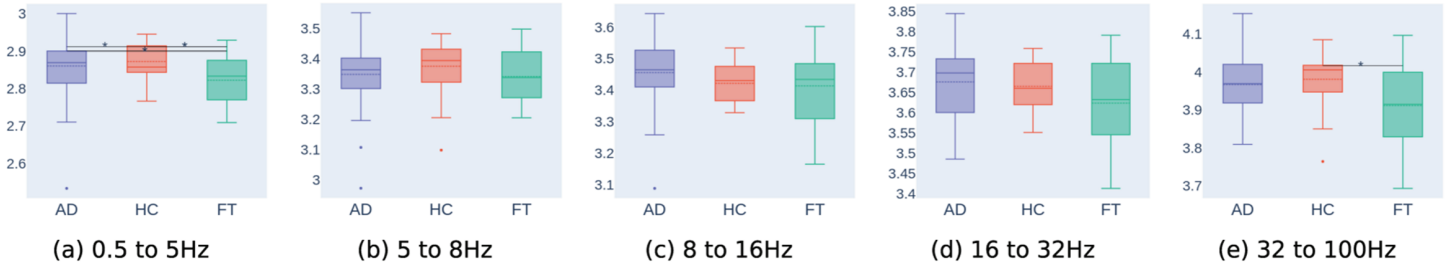

Fig 22. Box plot of the Shannon entropy of the information rate distribution in the temporal region (AD: Alzheimer's disease; HC: healthy controls; FT: frontotemporal dementia). Significant differences ($p<0.05$) are indicated by "–*–".

https://doi.org/10.1371/journal.pcsy.0000059.g022

assess the 'spread' of each participant's information rate distribution. The summarized findings based on the information rate distribution are detailed in Table 2. Also, the asymmetry in EEG dynamics between the left and right temporal regions is observed specifically in the Alzheimer's group as shown in Fig 23. Furthermore, for the second dataset, the mean, skewness, and kurtosis of the information rate distribution can effectively distinguish between the healthy and MCI groups through the frontal and temporal regions as shown in Figs 24, 25, 26, 27 and summarized in Table 3.

Table 2. Frequency bands that show significant difference based on Shannon entropy and statistical moments of the distribution of information rate. The result is based on the first dataset that consists of Alzheimer's, frontotemporal dementia, and Healthy subjects [39].

region	Shannon entropy	mean	variance	skewness	kurtosis
frontal	θ (A-C-D), α (C-D), β (C-D), γ (A-C-D)	θ (A-C)	θ (A-C)	θ (A-C)	θ (A-C)
central	δ (C-D), γ (A-C-D)	\	θ (A-C)	\	\
parietal	α (A-D), γ (C-D)	α (A-C), β (A-C)	\	β (A-C)	β (A-C)
occipital	\	α (A-C-D), β (A-C)	\	α (A-C), β (A-C-D)	α (A-C), β (A-C)
temporal	δ (A-C-D), γ (C-D)	α (A-C-D)	α (A-C)	α (A-C-D)	α (A-C-D)

The frequency bands shown here are δ (0.5 to 5 Hz), θ (5 to 8 Hz), α (8 to 16 Hz), β (16 to 32 Hz), and γ (32 to 100 Hz). The groups of Alzheimer's, Healthy, and frontotemporal dementia are indicated as A, C, and D, respectively. The groups showing significant differences (p<0.05) after Kruskal-Wallis and Dunn's test are labelled in the brackets. For instance, A-C indicates a significant difference between the Alzheimer's and Healthy groups. A-C-D denotes significant differences among all groups, while \ indicates no combination showing significant differences. The results shown here are summarized based on Figs 4, 5, 6, 7, 8, 9, 10, 11, 12, 13, 14, 15, 16, 17, 18, 19, 20, 21, and 22.

https://doi.org/10.1371/journal.pcsy.0000059.t002

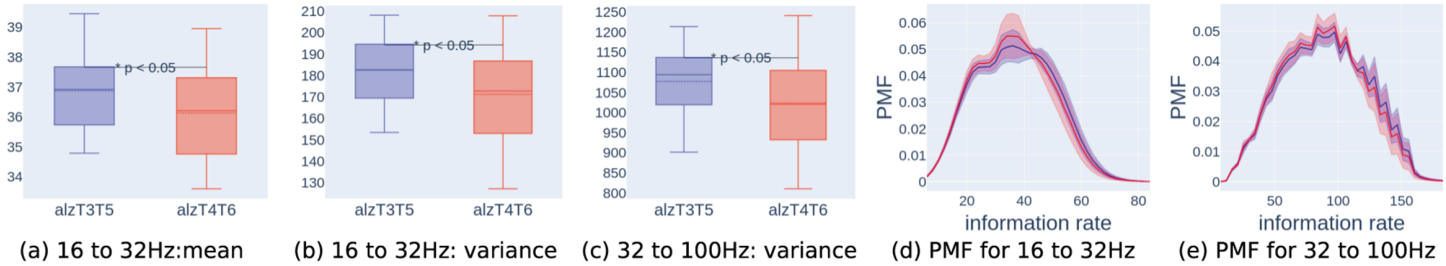

Fig 23. Significant difference (p<0.05) for asymmetry study of temporal region based on statistical moments of information rate distribution for Alzheimer's participants shown in (a) to (c). The correspond distributions are shown in (d) and (e). Note blue is the left region and red is right region.

https://doi.org/10.1371/journal.pcsy.0000059.g023

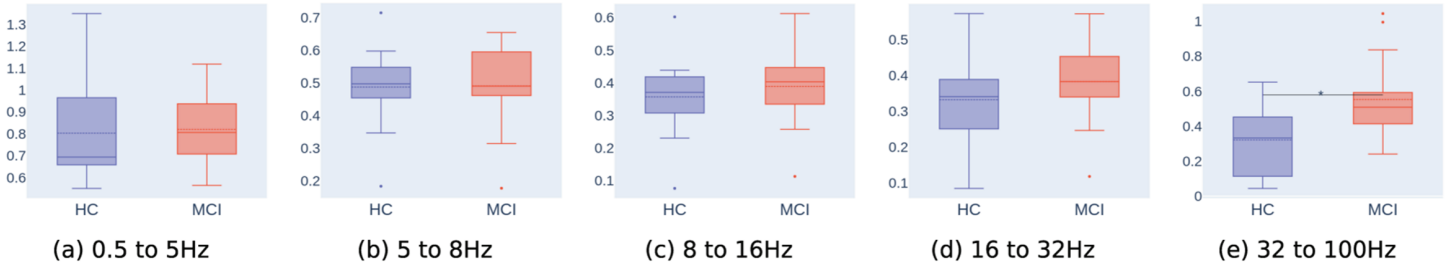

Fig 24. Box plot of the skewness of the information rate distribution in the frontal region (HC: healthy controls; MCI: Mild Cognitive Impairment). Significant differences (p<0.05) are indicated by "–*–".

https://doi.org/10.1371/journal.pcsy.0000059.g024

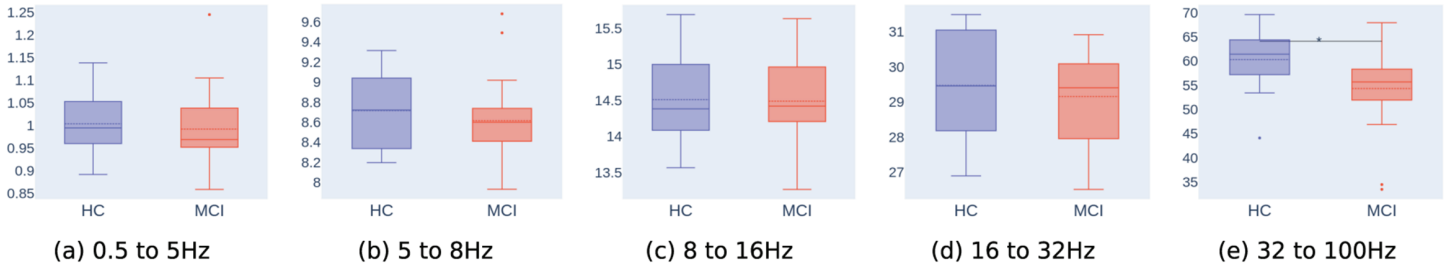

Fig 25. Box plot of the mean of the information rate distribution in the temporal region (HC: healthy controls; MCI: Mild Cognitive Impairment). Significant differences (p<0.05) are indicated by "–*–".

https://doi.org/10.1371/journal.pcsy.0000059.g025

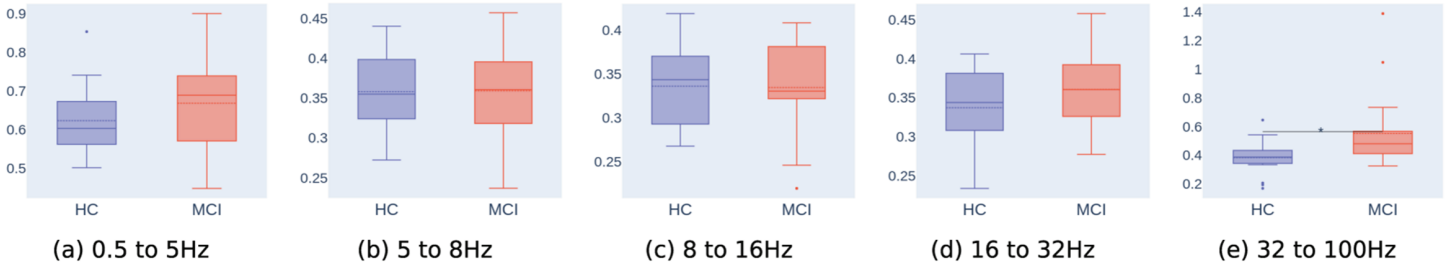

Fig 26. Box plot of the skewness of the information rate distribution in the temporal region (HC: healthy controls; MCI: Mild Cognitive Impairment). Significant differences (p<0.05) are indicated by "–*–".

https://doi.org/10.1371/journal.pcsy.0000059.g026

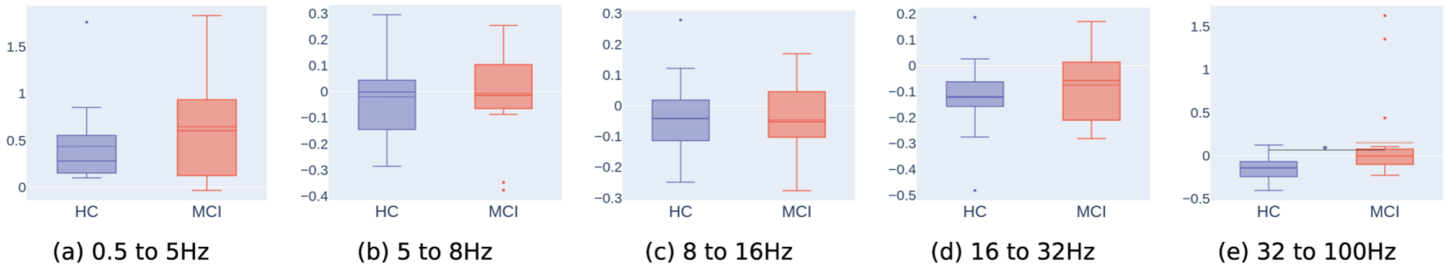

Fig 27. Box plot of the Kurtosis of the information rate distribution in the temporal region (HC: healthy controls; MCI: Mild Cognitive Impairment). Significant differences (p<0.05) are indicated by "–*–".

https://doi.org/10.1371/journal.pcsy.0000059.g027

Table 3. Frequency bands that show significant difference based on Shannon entropy and statistical moments of the distribution of information rate. The result is based on the second dataset that consists of Mild Cognitive Impairment and Healthy subjects [40]

region	Shannon entropy	mean	variance	skewness	kurtosis
frontal	\	\	\	γ (M-C)	\
central	\	\	\	\	\
parietal	\	\	\	\	\
occipital	\	\	\	\	\
temporal	\	γ (M-C)	\	γ (M-C)	γ (M-C)

The frequency bands shown here are δ (0.5 to 5 Hz), θ (5 to 8 Hz), α (8 to 16 Hz), β (16 to 32 Hz), and γ (32 to 100 Hz). The groups of Healthy and Mild Cognitive Impairment (MCI) are indicated as C and M, respectively. The groups showing significant differences (p<0.05) after Kruskal-Wallis and Dunn's test are labelled in the brackets. For instance, M-C indicates a significant difference between the MCI and Healthy groups, while \ indicates no combination showing significant differences. The results shown here are summarized based on Figs 24, 25, 26, and 27.

https://doi.org/10.1371/journal.pcsy.0000059.t003

Discussion

Based on the box plots of the information rate's mean, variance, skewness, and kurtosis, the frontal region generally demonstrates significant differences ($p<0.05$) that allow for differentiation of the Alzheimer's and healthy group at the theta band (5 to 8 Hz). This trend is clearly visible in S12 Fig(b). This finding aligns with our hypothesis in the introduction, which was motivated by prior descriptions suggesting that Alzheimer's disease and frontotemporal dementia are associated with reduced complexity or itinerancy in neuronal dynamics. Such a reduction reflects a decline in the brain's ability to explore diverse functional states, resulting in a lower information rate and diminished variability across time — particularly in regions like the frontal cortex, which are most affected by these disorders. We, therefore, anticipated a reduction in the mean and variance of the information rate in these patient groups and expected that these alterations would manifest across multiple frequency bands in a scale-invariant manner. Generally, the reductions of mean and variance in information rate can be observed through the mean (dotted line within the box) and median (solid line within the box) of the box plots shown Figs 4 and 8. Although the distribution of information rate at central region exhibits visual differences at the theta band between the groups, as shown in S13 Fig(b) only variance (see Fig 9(b)) reflects a significant difference among groups, while the mean, skewness, and kurtosis do not show such distinctions.

In the parietal region, the distributions shown in S14 Fig(b) indicate that healthy and frontotemporal participants tend to exhibit higher information rates than Alzheimer's participants. However, the high variability in the distributions among participants limits statistical significance, making it difficult to differentiate the groups. Conversely, in the beta band (16 to 32 Hz), the mean, skewness, and kurtosis show significant differences between the Alzheimer's and healthy groups, as shown in Fig 5(d), Fig 12(d), and Fig 16(d). Additionally, at the alpha band (8 to 16 Hz), significant differences in mean of information rate are observed between Alzheimer's and healthy groups (Fig 5(c)). This finding only aligns with our hypothesis at the delta band (0.5 to 5 Hz) and theta band (5 to 8 Hz), in which Alzheimer's and frontotemporal dementia groups have a lower mean of information rate than the healthy group as shown in Fig 5.

In the occipital region, both alpha and beta bands exhibit significant differences across all groups (Alzheimer's, healthy, and frontotemporal) based on mean and skewness, as displayed in Fig 6(c) and Fig13(d). In the alpha band, skewness and kurtosis reveal significant differences between the Alzheimer's and healthy groups, while in the beta band, kurtosis indicates significant differences between the healthy and frontotemporal groups. For the temporal region, the alpha band differentiates all groups based on mean, skewness, and kurtosis of the information rate, as illustrated in S16 Fig(c). However, variance in this region only differentiates Alzheimer's and healthy groups (Fig 10(c)). Similar to the parietal region, our hypothesis fails to align with the findings in the occipital region as only the delta band has the lower mean in information rate as shown in Fig 6(a).

Shannon entropy of the information rate distribution provides another method for characterizing differences among the groups. For instance, at the gamma band (32 to 100 Hz), the frontal and central regions show significant differences between groups, as seen in Fig 19(e) and Fig 20(e). In contrast, the parietal and temporal regions can only differentiate between healthy and frontotemporal groups (Fig 21(e) and Fig 22(e)). At the delta band (0.5 to 5 Hz), Shannon entropy of information rate distribution in the central region shows significant differences between healthy and frontotemporal groups (Fig 20(a)). Similarly, the frontal region exhibits significant differences between frontotemporal and healthy groups at the alpha and

beta bands (Fig 19(c) and Fig 19(d)). The frontal and temporal regions show significant differences across all groups at the theta and delta bands, respectively (Fig 19(b) and Fig 22(a)). Notably, Shannon entropy of information rate distribution reveals a significant difference between Alzheimer's and frontotemporal groups at the alpha band in the parietal region (Fig 21(c)), while the occipital region shows no significant differences in Shannon entropy among groups (Fig 20), which aligns with the results from the Jensen-Shannon distance comparison in Table 1.

Based on the results from statistical moments of the information rate, it is evident that theta, alpha, and beta bands serve as effective frequency bands for differentiating between the groups. As previously noted, all statistical moments are able to distinguish at least the Alzheimer's and healthy groups across regions, with the exception of the occipital region at the beta band, where only the healthy and frontotemporal dementia groups are distinguishable. Additionally, the frontal and temporal regions exhibit significant differences in all statistical moments at the theta and alpha bands, respectively. These findings align closely with those in Table 1, where a high proportion (> 50%) of Jensen-Shannon distance combinations demonstrated significant combination differences following the Kruskal-Wallis test. Similarly, in the parietal region, the alpha and beta bands can differentiate at least between Alzheimer's and healthy groups, showing trends consistent with Table 1. However, at the alpha and beta bands, the occipital region effectively differentiates groups based on the statistical moments of the information rate distribution, a distinction not observed in Table 1. This suggests the presence of dynamic differences in EEG signals within the occipital region, as information rate captures the evolution of signals based on amplitude variations in that region, which may not be apparent in average values presented in Table 1.

Furthermore, while Table 1 reveals a number of significant combinations for delta and gamma bands in distinguishing groups, the statistical moments of the information rate suggest otherwise. This discrepancy may imply that, although signal dynamics are similar across brain regions among groups, there are underlying amplitude differences, as suggested by pairwise Jensen-Shannon distance comparisons in Table 1.

Shannon entropy of the information rate distribution primarily differentiates healthy participants from the frontotemporal dementia group, as noted. Notably, the frontal region can distinguish between these groups across the theta, alpha, beta, and gamma bands. Shannon entropy of the gamma band's information rate distribution proves generally useful across all brain regions, except the occipital, in identifying the frontotemporal dementia group. This may be due to the high variability in the information rate distribution for the frontotemporal dementia group within this small dataset. Although variance quantifies the spread of a distribution, it does not yield results analogous to Shannon entropy in statistical tests (see Table 2) because variance is inherently tied to the mean of the distribution, while Shannon entropy measures uncertainty without reference to the mean.

Moreover, the information rate effectively reveals the asymmetry in the dynamics of EEG signals between the left (electrodes: T3 and T5) and right (electrodes: T4 and T6) temporal regions in Alzheimer's participants. As shown in Fig 23, there are significant differences between the left and right temporal regions at the beta and gamma bands. Visually, the variance for the left region appears to be larger than that for the right, as depicted in Fig 23(d) and Fig 23(e). This observation is confirmed by the statistical tests presented in Fig 23(b) and Fig 23(c). Additionally, there is a significant difference in the mean of information rates between the left and right temporal regions at the beta band, as shown in Fig 23(a), although this may not be clearly discernible from the PMFs presented in Fig 23(d) and Fig 23(e). Notably, this asymmetry is present only in the Alzheimer's group at these frequency bands, while it is absent in the frontotemporal dementia and healthy groups.

Additionally, the information rate distribution effectively distinguishes between the healthy and Mild Cognitive Impairment (MCI) groups in the gamma band for the second dataset, as shown in Figs 24, 25, 26, 27 and summarized in Table 3. The figures indicate that the healthy group tends to exhibit higher complexity in both the frontal and temporal regions, as depicted in the information rate distributions S17 Fig(e) and S18 Fig(e), compared to the MCI group. This is evident in the skewness of the box plots, where the healthy group shows significantly higher values than the MCI group, as shown in Fig 24(e) and Fig 26(e).

Moreover, the statistically significant difference in the mean of the information rate distribution in the temporal region further supports the observation that the healthy group exhibits greater complexity than the MCI group, as illustrated in Fig 25(e). Additionally, the kurtosis of the information rate distribution in the temporal region shows a statistically significant difference, with the healthy group having higher values than the MCI group, as presented in Fig 27(e) and visually confirmed in S18 Fig(e).

For future work, machine learning techniques could be explored to classify these participant groups based on statistical moments or Shannon entropy derived from the information rate distribution. As discussed, Shannon entropy of the information rate distribution effectively differentiates frontotemporal dementia patients from healthy participants, while statistical moments can distinguish between Alzheimer's and healthy groups. It is important to note that the findings here, obtained using the information rate technique to evaluate signal dynamics across brain regions, are specific to the dataset provided by [39]. A broader generalization of these findings would require further validation on additional datasets in future studies.

Conclusion

In conclusion, this study utilizes the complementary statistical methods and Shannon entropy of information rate distribution in differentiating Alzheimer's, frontotemporal dementia, and healthy participants based on EEG data across various brain regions as an ensemble and frequency bands. Theta, alpha, and beta bands emerged as particularly effective for distinguishing group differences, with statistical moments successfully differentiating Alzheimer's from healthy groups, particularly in the frontal and temporal regions. Additionally, Shannon entropy of the information rate demonstrated a distinctive capability in identifying frontotemporal dementia participants, especially in the frontal region across theta to gamma bands. This result underscores the value of exploring both amplitude and variability within EEG signals to gain insights into neurodegenerative patterns. Notably, information rate techniques in the occipital region indicated dynamic differences that may not be fully captured by traditional average-based analysis, suggesting the potential for enhanced diagnostic granularity through information rate measures. Moreover, this technique effectively demonstrates the left-right asymmetry in the dynamics of EEG signals in the temporal region that is observed in the Alzheimer's group. In addition,the information rate distribution is also able to distinguish the Mild Cognitive Impairment group from the healthy group—an outcome not achieved using the Jensen–Shannon distance.

These findings set a foundation for future research to develop machine learning models that could leverage these statistical moments and entropy-based metrics for more precise classification of neurodegenerative conditions. However, to broaden the applicability of these findings, validation on larger and more diverse datasets will be essential. Overall, the insights gained from this study contribute to the expanding field of quantitative EEG analysis, emphasizing the promise of using information rate-based approaches for improved differentiation and understanding of neurological disorders.

Supporting information

S1 Fig. Box plots of the Jensen-Shannon distance for the frontal region, showing significant differences after Kruskal-Wallis test at the delta band (0.5 to 5 Hz).
(EPS)

S2 Fig. Box plots of the Jensen-Shannon distance for the frontal region, showing significant differences after Kruskal-Wallis test at the theta band (5 to 8 Hz).
(EPS)

S3 Fig. Box plots of the Jensen-Shannon distance for the frontal region, showing significant differences after Kruskal-Wallis test at the gamma band (32 to 100 Hz).
(EPS)

S4 Fig. Jensen-Shannon distance of Central region with significant difference in Kruskal-Wallis at delta band (0.5 to 5 Hz).
(EPS)

S5 Fig. Box plots of the Jensen-Shannon distance for the parietal region, showing significant differences after Kruskal-Wallis test at the delta band (0.5 to 5 Hz).
(EPS)

S6 Fig. Box plots of the Jensen-Shannon distance for the parietal region, showing significant differences after Kruskal-Wallis test at the alpha band (8 to 16 Hz).
(EPS)

S7 Fig. Box plots of the Jensen-Shannon distance for the parietal region, showing significant differences after Kruskal-Wallis test at the beta band (16 to 32 Hz).
(EPS)

S8 Fig. Box plots of the Jensen-Shannon distance for the temporal region, showing significant differences after Kruskal-Wallis test at the theta band (5 to 8 Hz).
(EPS)

S9 Fig. Box plots of the Jensen-Shannon distance for the temporal region, showing significant differences after Kruskal-Wallis test at the alpha band (8 to 16 Hz).
(EPS)

S10 Fig. Jensen-Shannon distance of Temporal region with significant difference in Kruskal-Wallis at beta band (16 to 32 Hz).
(EPS)

S11 Fig. Box plots of the Jensen-Shannon distance for the temporal region, showing significant differences after Kruskal-Wallis test at the gamma band (32 to 100 Hz).
(EPS)

S12 Fig. Frontal region of information rate distribution (Blue: Alzheimer's, Red: healthy, Green: frontotemporal dementia).
(EPS)

S13 Fig. Central region of information rate distribution (Blue: Alzheimer's, Red: healthy, Green: frontotemporal dementia).
(EPS)

S14 Fig. Parietal region of information rate distribution (Blue: Alzheimer's, Red: healthy, Green: frontotemporal dementia).
(EPS)

S15 Fig. Occipital region of information rate distribution (Blue: Alzheimer's, Red: healthy, Green: frontotemporal dementia).
(EPS)

S16 Fig. Temporal region of information rate distribution (Blue: Alzheimer's, Red: healthy, Green: frontotemporal dementia).
(EPS)

S17 Fig. Frontal region of information rate distribution (Red: healthy, Green: Mild Cognitive Impairment).
(EPS)

S18 Fig. Temporal region of information rate distribution (Red: healthy, Green: Mild Cognitive Impairment).
(EPS)

Acknowledgments

This work was supported by UK Research and Innovation under the EPSRC grant EP/X020193/1, awarded to Fei He (https://gtr.ukri.org/projects?ref=EP%2FX020193%2F1). The funder had no role in study design, data collection and analysis, decision to publish, or preparation of the manuscript.

Author contributions

Conceptualization: Heng Jie Choong, Eun-jin Kim.

Formal analysis: Heng Jie Choong.

Funding acquisition: Eun-jin Kim, Fei He.

Investigation: Heng Jie Choong, Eun-jin Kim, Fei He.

Methodology: Heng Jie Choong, Eun-jin Kim.

Resources: Heng Jie Choong.

Software: Heng Jie Choong.

Supervision: Eun-jin Kim, Fei He.

Validation: Heng Jie Choong, Eun-jin Kim, Fei He.

Writing – original draft: Heng Jie Choong.

Writing – review & editing: Heng Jie Choong, Eun-jin Kim, Fei He.

References

1. Nardone R, Sebastianelli L, Versace V, Saltuari L, Lochner P, Frey V, et al. Usefulness of EEG techniques in distinguishing frontotemporal dementia from alzheimer's disease and other dementias. Dis Markers. 2018;2018:6581490. https://doi.org/10.1155/2018/6581490 PMID: 30254710
2. Arvanitakis Z, Shah RC, Bennett DA. Diagnosis and management of dementia: review. JAMA. 2019;322(16):1589–99. https://doi.org/10.1001/jama.2019.4782 PMID: 31638686
3. Aging NI. Understanding different types of dementia. 2023. https://www.nia.nih.gov/health/alzheimers-and-dementia/understanding-different-types-dementia
4. Kinaan JA, Reddy V, Lui AF. Neuroanatomy, Cerebral Cortex. In: StatPearls [internet]. StatPearls Publishing; 2023.

5. St Louis EK, Frey LC, Britton JW. Electroencephalography (EEG): an introductory text and atlas of normal and abnormal findings in adults, children, and infants. Chicago: American Epilepsy Society; 2016.
6. Abhang PA, Gawali BW, Mehrotra SC. Technological basics of EEG recording and operation of apparatus. Introduction to EEG- and speech-based emotion recognition. Elsevier; 2016. p. 19–50. https://doi.org/10.1016/b978-0-12-804490-2.00002-6
7. Warren SL, Moustafa AA. Functional magnetic resonance imaging, deep learning, and Alzheimer's disease: a systematic review. J Neuroimaging. 2023;33(1):5–18. https://doi.org/10.1111/jon.13063 PMID: 36257926
8. Sperling R. Potential of functional MRI as a biomarker in early Alzheimer's disease. Neurobiol Aging. 2011;32(Suppl 1):S37-43. https://doi.org/10.1016/j.neurobiolaging.2011.09.009 PMID: 22078171
9. Yen C, Lin C-L, Chiang M-C. Exploring the frontiers of neuroimaging: a review of recent advances in understanding brain functioning and disorders. Life (Basel). 2023;13(7):1472. https://doi.org/10.3390/life13071472 PMID: 37511847
10. Daly I, Williams D, Hwang F, Kirke A, Miranda ER, Nasuto SJ. Electroencephalography reflects the activity of sub-cortical brain regions during approach-withdrawal behaviour while listening to music. Sci Rep. 2019;9(1):9415. https://doi.org/10.1038/s41598-019-45105-2 PMID: 31263113
11. Saffari F, Norouzi K, Bruni LE, Zarei S, Ramsøy TZ. Impact of varying levels of mental stress on phase information of EEG signals: a study on the frontal, central, and parietal regions. Biomed Signal Process Control. 2023;86:105236. https://doi.org/10.1016/j.bspc.2023.105236
12. Crosson B, Ford A, Mcgregor KM, Meinzer M, Cheshkov S, Li X, et al. Functional imaging and related techniques: an introduction for rehabilitation researchers. J Rehabilit Res Develop. 2010.
13. Zheng X, Wang B, Liu H, Wu W, Sun J, Fang W, et al. Diagnosis of Alzheimer's disease via resting-state EEG: integration of spectrum, complexity, and synchronization signal features. Front Aging Neurosci. 2023;15:1288295. https://doi.org/10.3389/fnagi.2023.1288295 PMID: 38020761
14. Kopčanová M, Tait L, Donoghue T, Stothart G, Smith L, Flores-Sandoval AA, et al. Resting-state EEG signatures of Alzheimer's disease are driven by periodic but not aperiodic changes. Neurobiol Dis. 2024;190:106380. https://doi.org/10.1016/j.nbd.2023.106380 PMID: 38114048
15. Adamis D, Sahu S, Treloar A. The utility of EEG in dementia: a clinical perspective. Int J Geriatr Psychiatry. 2005;20(11):1038–45. https://doi.org/10.1002/gps.1393 PMID: 16250070
16. Claus JJ, Ongerboer de Visser BW, Walstra GJ, Hijdra A, Verbeeten B Jr, van Gool WA. Quantitative spectral electroencephalography in predicting survival in patients with early Alzheimer disease. Arch Neurol. 1998;55(8):1105–11. https://doi.org/10.1001/archneur.55.8.1105 PMID: 9708961
17. Jelic V, Johansson SE, Almkvist O, Shigeta M, Julin P, Nordberg A, et al. Quantitative electroencephalography in mild cognitive impairment: longitudinal changes and possible prediction of Alzheimer's disease. Neurobiol Aging. 2000;21(4):533–40. https://doi.org/10.1016/s0197-4580(00)00153-6 PMID: 10924766
18. Kim E-J. Information geometry, fluctuations, non-equilibrium thermodynamics, and geodesics in complex systems. Entropy (Basel). 2021;23(11):1393. https://doi.org/10.3390/e23111393 PMID: 34828093
19. Kim E. Information geometry and non-equilibrium thermodynamic relations in the over-damped stochastic processes. J Stat Mech. 2021;2021(9):093406. https://doi.org/10.1088/1742-5468/ac21d6
20. Hua J-C, Kim E-J, He F. Information geometry theoretic measures for characterizing neural information processing from simulated EEG signals. Entropy (Basel). 2024;26(3):213. https://doi.org/10.3390/e26030213 PMID: 38539727
21. Safi MS, Safi SMM. Early detection of Alzheimer's disease from EEG signals using Hjorth parameters. Biomed Signal Process Control. 2021;65:102338. https://doi.org/10.1016/j.bspc.2020.102338
22. Hjorth B. EEG analysis based on time domain properties. Electroencephalogr Clin Neurophysiol. 1970;29(3):306–10. https://doi.org/10.1016/0013-4694(70)90143-4 PMID: 4195653
23. Rohila A, Sharma A. Phase entropy: a new complexity measure for heart rate variability. Physiol Meas. 2019;40(10):105006. https://doi.org/10.1088/1361-6579/ab499e PMID: 31574498
24. Bandt C, Pompe B. Permutation entropy: a natural complexity measure for time series. Phys Rev Lett. 2002;88(17):174102. https://doi.org/10.1103/PhysRevLett.88.174102 PMID: 12005759
25. Shi W, Shang P, Lin A. The coupling analysis of stock market indices based on cross-permutation entropy. Nonl Dyn. 2014;79(4):2439–47. https://doi.org/10.1007/s11071-014-1823-1
26. Delgado-Bonal A, Marshak A. Approximate entropy and sample entropy: a comprehensive tutorial. Entropy (Basel). 2019;21(6):541. https://doi.org/10.3390/e21060541 PMID: 33267255

27. Li P, Liu C, Li K, Zheng D, Liu C, Hou Y. Assessing the complexity of short-term heartbeat interval series by distribution entropy. Med Biol Eng Comput. 2015;53(1):77–87. https://doi.org/10.1007/s11517-014-1216-0 PMID: 25351477
28. Jeong J. EEG dynamics in patients with Alzheimer's disease. Clin Neurophysiol. 2004;115(7):1490–505. https://doi.org/10.1016/j.clinph.2004.01.001 PMID: 15203050
29. Al-Qazzaz NK, Ali SHBM, Ahmad SA, Chellappan K, Islam MS, Escudero J. Role of EEG as biomarker in the early detection and classification of dementia. ScientificWorldJournal. 2014;2014:906038. https://doi.org/10.1155/2014/906038 PMID: 25093211
30. Brown CW, Chen H-Y, Panegyres PK. Electroencephalography in young onset dementia. BMC Neurol. 2023;23(1). https://doi.org/10.1186/s12883-023-03248-w
31. Babiloni C, Ferri R, Binetti G, Vecchio F, Frisoni GB, Lanuzza B, et al. Directionality of EEG synchronization in Alzheimer's disease subjects. Neurobiol Aging. 2009;30(1):93–102. https://doi.org/10.1016/j.neurobiolaging.2007.05.007 PMID: 17573161
32. Henderson G, Ifeachor E, Hudson N, Goh C, Outram N, Wimalaratna S, et al. Development and assessment of methods for detecting dementia using the human electroencephalogram. IEEE Trans Biomed Eng. 2006;53(8):1557–68. https://doi.org/10.1109/TBME.2006.878067 PMID: 16916090
33. de Waal H, Stam CJ, Blankenstein MA, Pijnenburg YAL, Scheltens P, van der Flier WM. EEG abnormalities in early and late onset Alzheimer's disease: understanding heterogeneity. J Neurol Neurosurg Psychiatry. 2011;82(1):67–71. https://doi.org/10.1136/jnnp.2010.216432 PMID: 20935323
34. Tononi G, Sporns O, Edelman GM. A measure for brain complexity: relating functional segregation and integration in the nervous system. Proc Natl Acad Sci U S A. 1994;91(11):5033–7. https://doi.org/10.1073/pnas.91.11.5033 PMID: 8197179
35. Fries P. Neuronal gamma-band synchronization as a fundamental process in cortical computation. Annu Rev Neurosci. 2009;32:209–24. https://doi.org/10.1146/annurev.neuro.051508.135603 PMID: 19400723
36. Poza J, Gómez C, García M, Bachiller A, Fernández A, Hornero R. Analysis of spontaneous MEG activity in mild cognitive impairment and Alzheimer's disease using Jensen's divergence. Annu Int Conf IEEE Eng Med Biol Soc. 2014;2014:1501–4. https://doi.org/10.1109/EMBC.2014.6943886 PMID: 25570254
37. Zhang ZX, Xu SQ, Zhou EN, Huang XL, Wang J. Alpha wave attention EEG analysis based on the multiscale jensen-shannon divergence. AMM. 2014;595:269–73. https://doi.org/10.4028/www.scientific.net/amm.595.269
38. Gong L, Wang J. Complexity analysis of electroencephalogram signal based on Jensen-Shannon divergence. In: 2013 6th International Conference on Biomedical Engineering and Informatics. 2013. p. 219–23. https://doi.org/10.1109/bmei.2013.6746937
39. Miltiadous A, Tzimourta KD, Afrantou T, Ioannidis P, Grigoriadis N, Tsalikakis DG, et al. A dataset of scalp EEG recordings of Alzheimer's disease, frontotemporal dementia and healthy subjects from routine EEG. Data. 2023;8(6):95. https://doi.org/10.3390/data8060095
40. EEG Signals From Normal and Mild Cognitive Impairment (MCI) Cases. [cited 2023 Oct 1]. https://misp.mui.ac.ir/en/eeg-data-0
41. Nielsen F. On the Jensen–Shannon symmetrization of distances relying on abstract means. Entropy. 2019;21(5):485. https://doi.org/10.3390/e21050485
42. Ostertagová E, Ostertag O, Kováč J. Methodology and application of the Kruskal-Wallis test. AMM. 2014;611:115–20. https://doi.org/10.4028/www.scientific.net/amm.611.115
43. Kashefpoor M, Rabbani H, Barekatain M. Automatic diagnosis of mild cognitive impairment using electroencephalogram spectral features. J Med Signals Sens. 2016;6(1):25–32. https://doi.org/10.4103/2228-7477.175869 PMID: 27014609
44. Lee TW, Girolami M, Sejnowski TJ. Independent component analysis using an extended infomax algorithm for mixed subgaussian and supergaussian sources. Neural Comput. 1999;11(2):417–41. https://doi.org/10.1162/089976699300016719 PMID: 9950738
45. Sanchez-Reyes L-M, Rodriguez-Resendiz J, Avecilla-Ramirez GN, Garcia-Gomar M-L, Robles-Ocampo J-B. Impact of EEG parameters detecting dementia diseases: a systematic review. IEEE Access. 2021;9:78060–74. https://doi.org/10.1109/access.2021.3083519
46. Dubitzky W, Wolkenhauer O, Cho KH, Yokota H. Encyclopedia of systems biology. New York, NY: Springer; 2013.
47. Dinno A. Nonparametric pairwise multiple comparisons in independent groups using Dunn's Test. Stata J: Promot Commun Statistics Stata. 2015;15(1):292–300. https://doi.org/10.1177/1536867x1501500117